LA-UR- 09-06415

Approved for public release;
distribution is unlimited.

Title:	Strain Sensors for High Field Pulse Magnets
Author(s):	Christian Martinez, LANL, INST-OFF Yan Zheng, LANL, INST-OFF Daniel Easton, LANL, INST-OFF Kevin Farinholt, LANL, INST-OFF Gyuhae Park, LANL, INST-OFF
Intended for:	IMAC XXVII - A CONFERENCE AND EXPOSITION ON STRUCTURAL DYNAMICS

Form 836 (7/06)

Strain Sensors for High Field Pulse Magnets

Christian Martinez[1], Yan Zheng[2], Daniel Easton[3], Kevin Farinholt[4], Gyuhae Park[4]

[1]Dept. of Mechanical Engineering, Rice University, Houston, TX 77005
[2]Dept. Civil Engineering, Georgia Institute of Technology, Atlanta, GA, 30332
[3]Atomic Weapons Establishment plc, UK
[4]Engineering Institute, Los Alamos, National Laboratory, Los Alamos, NM 87545

ABSTRACT

In this paper we present an investigation into several strain sensing technologies that are being considered to monitor mechanical deformation within the steel reinforcement shells used in high field pulsed magnets. Such systems generally operate at cryogenic temperatures to mitigate heating issues that are inherent in the coils of nondestructive, high field pulsed magnets. The objective of this preliminary study is to characterize the performance of various strain sensing technologies at liquid nitrogen temperatures (-196°C). Four sensor types are considered in this investigation: fiber Bragg gratings (FBG), resistive foil strain gauges (RFSG), piezoelectric polymers (PVDF), and piezoceramics (PZT). Three operational conditions are considered for each sensor: bond integrity, sensitivity as a function of temperature, and thermal cycling effects. Several experiments were conducted as part of this study, investigating adhesion with various substrate materials (stainless steel, aluminum, and carbon fiber), sensitivity to static (FBG and RFSG) and dynamic (RFSG, PVDF and PZT) load conditions, and sensor diagnostics using PZT sensors. This work has been conducted in collaboration with the National High Magnetic Field Laboratory (NHMFL), and the results of this study will be used to identify the set of sensing technologies that would be best suited for integration within high field pulsed magnets at the NHMFL facility.

1. INTRODUCTION

High field, multi-pulse magnets are very useful in materials and physics related research. These systems produce magnetic fields of 60-100 Tesla for periods of 15 ms or longer. Such fields are larger than those provided by continuous field magnets, yet without the single-shot limitations of high field, explosively driven destructive magnets. Continuous field magnets are capable of sustaining fields of 45 Tesla, whereas the recently developed 100T multi-shot system at the National High Magnetic Field Laboratory (NHMFL) at Los Alamos National Laboratory (LANL) has reach a record field of 90Tesla, and is currently being conditioned toward the operational goal of 100 Tesla. The 100T multi-shot magnet is composed of a two stage design. The outer stage of this system is composed of a series of six nested, resistive, solenoid coils that are driven by a 1,400 MW generator to provide platform fields of 40 Tesla. This outer stage surrounds an 'insert' composed of eleven superconducting coils that are powered by a 1.4 MJ, 18kV capacitor bank to produce a nominal field of 60 Tesla [1]. The duration of this pulsed field is 15ms, and is shown in Figure 1. A schematic of how the insert and outer stage are configured for the 100T system is shown in Figure 2. Each coil in the outer stage of this system are fit inside Nitronic-40™ stainless steel reinforcement shells that provide structural support due to the large radial forces that develop during each pulse cycle. Such forces often stress these reinforcement shells to their material limits with strains approaching 1% in the center coils. In addition to the severe electrical and mechanical

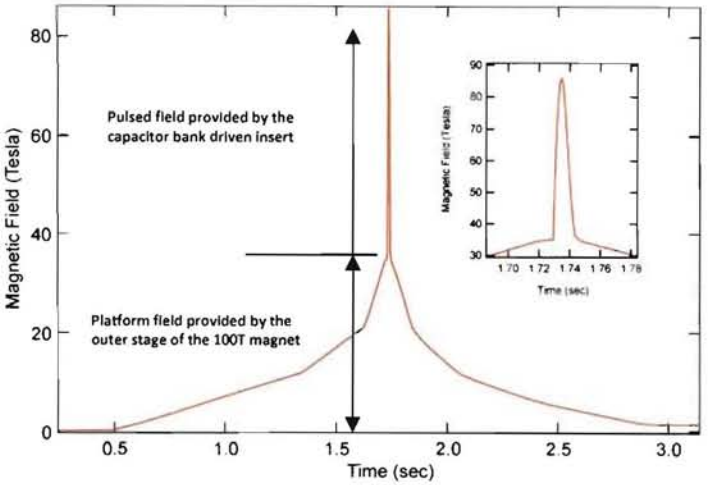

Figure 1: Magnetic field profile generated by the 100 Tesla multi-pulse magnet.

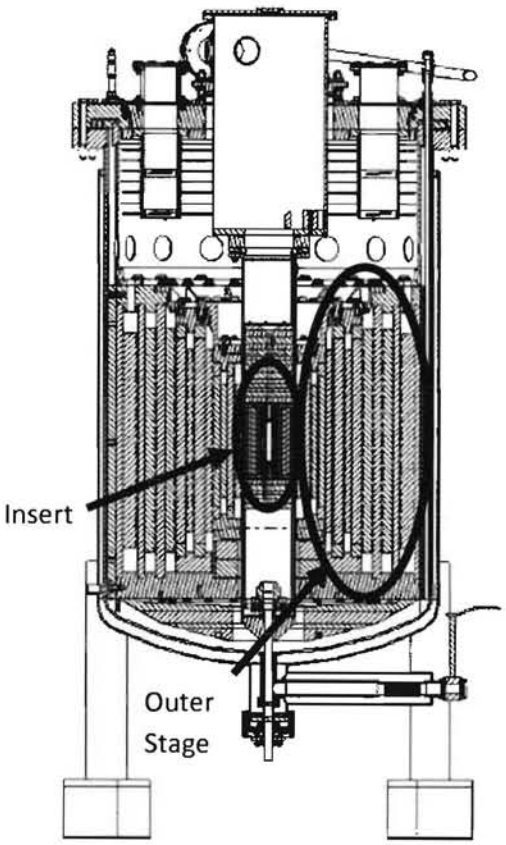

Figure 2: Schematic of the shell and coil components of the 100 Tesla multi-pulse magnet.

environments produced in these large field magnets, the system must also operate at cryogenic temperatures to address heating issues and promote the superconducting properties of the insert coils.

1.1 Background

In July 2000, the 60T long-pulse magnet at NHMFL underwent a catastrophic failure that destroyed the entire magnet. This failure occurred after performing only 914 pulses of the expected 10,000 pulse lifespan. The entire magnet was destroyed in the resulting explosion, taking less than 5ms to release an estimated 8-80 GW of power in the process [2]. After extensive forensic analysis, it was determined that the cause of this destructive failure was the improper heat treatment of the reinforcement shells surrounding coils six and seven of the magnet (the 60T is composed of a series of nine nested, resistive, solenoid coils). As scientists and engineers worked to identify the cause of this failure and to develop safeguards to prevent future accidents, they also identified the need for integrated sensing capabilities to monitor the mechanical response of the magnet during operation. A series of subsequent magnets were designed and built to address the use of new design principles to improve reliability and avoid future failures. First, a 65 T magnet was created to introduce the concept of two, nested solenoid coils connected electronically in series. Next, a 75 T added a new Cu-Nb conductor to provide uniform distribution of the insert coil's mid-plane stress and conductor heating. Subsequently, an 80 T was pushed to failure in which the phenomenon of axial electromagnetic buckling was discovered and winding the metal shells was found to alleviate this stress [3].

Presently, magnet operators utilize the electrical properties of the magnet coils is used to monitor residual strain within the magnet following each pulse. A near failure in the 100T magnet was recently avoided due to these measurements; however an official health monitoring approach has yet to be developed for these systems. The large magnetic field affects most traditional strain sensors, and the large temperature fluctuations cause adhesion and material fatigue issues. As this poses a significant design challenge for many sensing technologies, this paper focuses on temperature effects on fiber Bragg gratings (FBG), resistive foil strain gauges (RFSG), piezoelectric ceramics (PZT), and piezoelectric polymers (PVDF). A series of static and dynamic experiments were designed to investigate sensor bonding and response at liquid nitrogen temperatures (77 K). Several substrates are considered in this investigation, as well as methods for interrogating the bonding condition to delineate between sensor failure and structural failure.

1.2 Project Description

The purpose of the project is to investigate strain sensing techniques that can be used to monitor deformation within the steel reinforcing shells (Figure 2) of a pulse magnet during operation. Due to the quick nature of these pulses, strain sensors identifying mechanical anomalies are needed to possibly prevent catastrophic failure. The high-field pulse magnets operate at the yield point of these structural materials, making full comprehension of deformation paramount to understanding the system's structural health. During use, the shells of the large magnet deform both axially and radially along the centerline of the structure. Currently, a resistive measurement method is being used to identify mechanical failure within the structure. However, this test gives little information as to the location of the failure as it is integrated over the length of each coil, making it difficult to monitor the life and reliability of individual components. This project works to identify appropriate adhesives that will bond to the stainless steel shells despite the large thermal gradient between cryogenic and room temperatures. It will also test the effect of the extreme temperature environment on RFSG, FBG, PZT and PVDF based sensors. By doing so, this project hopes to uncover a reasonable method of measuring strain within the magnet that can be easily implemented.

2. STRAIN SENSORS

In this study four strain sensing technologies are investigated: traditional resistive foil strain gauges, fiber Bragg gratings, piezoelectric ceramics and piezoelectric polymers. While each of these materials has the ability to measure dynamic strain, the optical hardware used in this study was limited to dynamic ranges below 1Hz. Therefore, tests were divided into two categories: static strain measurements using RFSG and FBG sensors, and dynamic strain measurements using RFSG, PZT, and PVDF sensors. The following section provides an overview of each type of sensor and considerations regarding their use in this application.

2.1 Resistive Foil Strain Gauges (RFSGs)

Foil resistive strain gauges are the most commonly used strain gauge types. RFSGs quantify strain by the measuring the mechanical deformation of a foil strip under strain. Under a tensile load, the cross-sectional geometry of the foil strip is deformed, resulting in a change in the resistance of the foil. This change in resistance directly affects the measured voltage through the foil, and so the strain can be derived from this change [4]. As RFSGs use electrical properties of the foil to measure strain, they are highly affected by electromagnetic fields, which induce currents that are not related to strain. It is possible that once the induced current has been measured, it can be subtracted from future readings. As RFSGs rely on the mechanical properties of the foil, they are also highly susceptible to changes in temperature. Bridge circuits that normalize the output, taking temperature changes into account with a dummy gauge, can be used to compensate for this affect.

2.2 Fiber Bragg Grating (FBG)

Fiber Bragg grating is an optical strain sensor that quantifies strain by measuring the wavelength of reflected light. The FBG is a small region of the optical fiber where the fiber core has been treated with a laser to produce a periodic modulation of its refractive index. The separation of each period of this modulation is referred to as the Bragg wavelength [5]. An infrared light is sent down the fiber optic strand and the strain is measured at the FBG sections of the fiber [6]. As the light from the LED hits the grating, only the wavelengths of light that correspond to the Bragg wavelength, that is the separation distances in the FBG, are allowed to be reflected back to the sensor. However, when the fiber strand is deformed as result of external

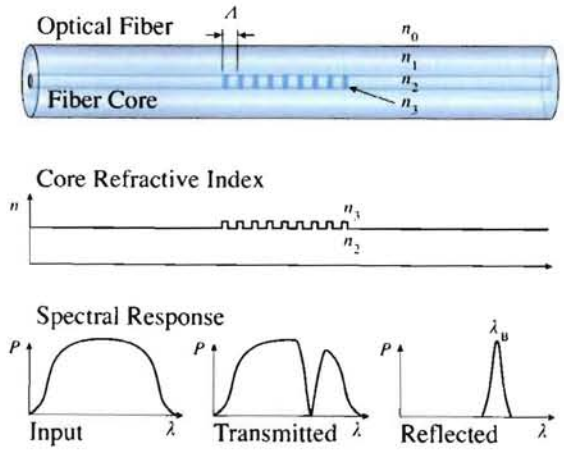

Figure 3: Schematic of how a Bragg grating functions.

strain, the Bragg wavelength will be increased, allowing for different wavelengths of light to be reflected back. The measured strain can be directly derived from the change in wavelengths of the light reflected from the Bragg grating. Different levels of strain applied to the fiber optic strand will allow a different reflected wavelength, which will correlate to the strain in the material to which the fiber is bonded[4]. When using these gauges, it is vital to ensure that the mounting is effective, in order to measure true strain on the surface of the material. Because of the importance of this aspect, different mounting techniques will be investigated, concentrating on those that can withstand the thermal cycling of almost 200 degrees between pulses.

2.3 Piezoelectric Strain Gauge

An alternative method for strain measurement is the use of piezoelectric transducers. The molecular structure of piezoelectric materials provides a coupling of mechanical and electrical domains, meaning that the material produces a mechanical response to an applied electrical field, and vice-versa. [5] By measuring the charge generated in the piezoelectric material, the stress in the material can be calculated [7]. Piezoelectric materials can only be used for dynamic measurements, as in a static strained state they will have no electrical output. For this work, piezoelectric sheet materials will be used to measure strain. These gauges will measure the average strain across the region covered by the sensor's surface area. Piezoelectric strain sensors have been shown to have advantages of compactness, sensitivity over a large strain bandwidth, lightweight, low power consumption, and ease of integration into structural components.[5,7] It has been demonstrated that [5] it is feasible to use piezoelectric strain sensing to detect both degradation of the mechanical and electrical properties of a piezoelectric gauge, and bonding defects between a piezoelectric gauge and the structure.

3. SENSOR DIAGNOSTICS

One component of this study is the reliability of sensor self-diagnostics at cryogenic temperatures. Due to the active nature of piezoelectric sensors, they can be used to actively interrogate the bonding and health condition of the sensor itself. Methods for determining the health of PZT transducers has been examined in previous research, however it has yet been demonstrated at extreme temperature environments. Saint-Pierre et al. uses the shape of the first real impedance resonance and its change to determine the state of the bonding condition [8]. Guirgiutiu and Zagrai propose a similar technique using the attenuation of the first imaginary impedance resonance for damage detection [9]. Pacou et al. discusses the use of the shift of the first natural frequency of the piezoelectric patch before and after bonding as a possible method for determining bonding condition [10].

There are several disadvantages to the above methods. First, they are not sensitive to small debonding in the PZT. Secondly they all require relatively high frequency measurements to determine the bonded first natural frequency. A standard impedance analyzer can be used to make a measurement into the 600 kHz range and up, which is needed in these methods. Current SHM nodes that are used for the impedance based SHM are not able to make impedance measurements into that range.[15] This frequency requirement makes these techniques generally unsuitable for field deployment using currently available sensor nodes. Finally the absolute number of data points that need to be collected for sensor diagnosis is quite high compared to the method purposed in this paper. The higher number of data points demands more from the SHM node, which generally have very limited storage capacity and RAM.

Bhalla and Soh [11] suggest that the imaginary part of the admittance measurement is more sensitive to bonding conditions, and therefore could be useful in determining the bond health. This relationship was further developed by Park et al. [7, 12], who showed the initial relationship between bonding condition and the slope of the imaginary admittance measurement (susceptance). This technique is based on the electrical admittance (Y) measurement of a free PZT

$$Y_{free}(\omega) = i\omega \frac{wl}{t_c}(\varepsilon_{33}^{T}(1 - i\delta)), \tag{1}$$

where ω is angular frequency, i is the complex number-$1^{1/2}$, w is sample width, l is sample length, t_c is thickness, ε_{33}^T is strain at constaint stress and δ is dielectric loss tangent of the PZT material. When bonded to a substrate the bonding layer's effect on the electrical admittance takes the form,

$$Y_{bond}(\omega) = i\omega \frac{wl}{t_c}(\varepsilon_{33}^T(1-i\delta) - d_{31}^2 \overline{Y}_P^E), \quad (2)$$

where d_{31}^2 is the piezoelectric coupling constant and Y_P^E is the complex Young's modulus of the PZT material at zero electric field. Equations 1 and 2 show that the same PZT will have a different capacitive value from a free-free condition to a surface-bonded condition. The bonding of the sensor would cause a downward shift in the electrical admittance of the free PZT by a factor of

$$d_{31}^2 \overline{Y}_P^E. \quad (3)$$

This change in slope would allow for the health of the bonding condition and the physical health of the transducer to be assessed with a measurement of the susceptance [7].

4. EXPERIMENTAL PROCEDURE

Several experiments were conducted as part of this investigation. The overall objective was to identify how each strain sensor reacts to operating in a cryogenic environment, how sensitivities scale, and whether room temperature sensor diagnostic techniques remain valid when submerged in liquid nitrogen. The first series of experiments were conducted to expose beam specimen to an environment similar to that found in the 60T and 100T multi-shot magnets. Due to limited access to user magnets in the NHMFL facility some conditions could not be replicated identically, such as the large currents and magnetic fields supplied by the large scale magnets. Therefore the principal focus of this experiment was on sensor response in extreme thermal conditions. Initial consideration was given to understanding thermal shock effects on sensor response, however further examination indicated that the least intrusive point of instrumentation would be on the outer circumference of the reinforcement shells. And while the coils of the magnet can undergo large thermal cycles from 77K to ~ 200K during a 15ms pulse, the system is refilled with liquid nitrogen as soon as the magnet is de-energized. Initial calculations indicate that the outer surfaces of the reinforcement shells may see a thermal change of 20°C between pulses, which in most applications is negligible with respect to sensitivity changes.

Three separate experiments were conducted in this study. The first of these focused on the response of an instrumented fixed-fixed beam that was excited in the center of each sample (Figure 4). Each sample was 25.4mm x 304.8mm x 3.2mm in size with 254.0 mm between clamping fixtures. Three materials were considered for the test samples: 304 stainless steel, 6061 aluminum, and carbon fiber. A center hole was drilled in each sample to attach a stinger that provided both static and dynamic excitations. In the case of static deformations a 10-32 threaded rod was used as an adjustment screw to impose fixed deformations related to the number of turns. The deformations that were imposed ranged from 0.8mm to 4mm for the samples instrumented with FBG and RFSG sensors. For dynamic measurements, the stinger was attached to a Labworks, Inc. ET-132 electro-magnetic shaker that applied chirp and harmonic signals to the test samples. Chirp excitations ranged from 10 to 1000 Hz, and were used to characterize RFSG, PVDF, and PZT sensors. In

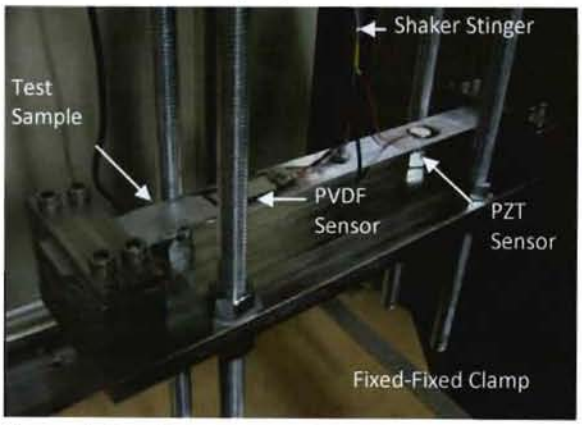

Figure 4: Test fixture used in fixed-fixed experiments. Samples were excited by an electromagnetic shaker.

each series of experiments samples were first tested at room temperature, then were submerged in a bath of liquid nitrogen (LiN) and allowed to cool to 77K. Once the samples were cooled, the nitrogen bath was lowered and samples were tested as they were suspended approximately 30mm above the LiN. The support stand and full setup are illustrated in Figure 5. In addition to the fixed-fixed condition, samples were tested in a free-free boundary condition by removing the clamping fixture. These tests focused on the dynamic response of the RFSG, PVDF and PZT samples as static deformations could not be imposed using the current test stand. As in the previous series of experiments, samples were first tested at room temperature, then lowered into the LiN bath and allowed to cool, then tested as they were suspended just above the LiN bath

Figure 5: Support stand used to suspend the clamping fixture and sample. Tests were conducted at room temperature and at cryogenic temperatures after the samples had been lowered into a liquid nitrogen bath.

Throughout these experiments data was acquired using three separate analyzers. The static tests using FBG relied on a Micron Optics sm125 Optical Sensing Interrogator to monitor the fiber Bragg grating, while data from RFSGs was collected using an Agilent 34970A BenchLink Data Logger with a Vishay P-3500 Strain Indicator used to provide appropriate signal conditioning. For dynamic tests a Dactron Photon signal analyzer was used to excite the structure and collect time and frequency domain data. Samples were driven in the fixed-fixed and free-free experiments with a Labworks ET-132 electromagnetic shaker and PA-135 amplifier. The reference signal for each test was obtained from a PCB208C03 force transducer mounted between the shaker and stinger attachment. ICP conditioning for the force transducer was supplied by the Dactron analyzer. Dynamic tests were conducted using a chirp excitation signal from 10-1000 Hz that was supplied over 80% of the acquisition window. Data was collected from up to 500 Hz through a hanning window. Each measurement consisted of 20 linear averages, and the beam's first natural frequency was identified and used as a harmonic excitation for the sample. This data was collected both at room temperature and LiN temperatures for each sample.

During the liquid nitrogen experiments the beam fixture was submerged in the LiN for approximately 10 minutes to ensure that the entire sample had equilibrated to 77K. Initial tests were conducted at this point while the sample remained under the liquid nitrogen solution. It was realized after these initial tests that the fluid was serving to mass load tests samples and provided increased damping in the system. To address this issue the test procedure was altered such that the bath of liquid nitrogen was lowered after the 10 minute cool down cycle so that the test sample was located approximately 30 mm above the surface of the LiN. This allowed the sample temperature to remain near 77K throughout the testing, while also removing the mass loading and damping influences attributed to submersion in the liquid nitrogen.

The final series of experiments conducted in this study considered the use of sensor diagnostics at cryogenic temperatures to interrogate bond health for piezoelectric ceramic sensors. In this test ten PZT sensors were bonded to an aluminum substrate using Stycast epoxy (Figure 6). One PZT sensor was unbonded and served as the control sensor in this experiment. Three PZTs were adhered to the aluminum substrate using even pressure and even coverage of epoxy to serve as a good bonding condition. Three sensors were bonded with wax paper cover small regions of the sensor (~ 3/8, 1/2 and 5/8 of the overall area) to provide a partial bonding condition. The final three sensors were bonded completely to the structure, then cut with an abrasive wheel to emulate varying degrees of damage (1/8, 1/4, and 1/2 removal of material). The test plate was suspended from the same test stand used in the

fixed-fixed and free-free experiments, and measurements were made at room temperature as well as in the LiN bath. The sensors were cycled through five cooling cycles, in which the plate was allowed to return to room temperature before being re-submerged in the LiN. Due to the high-frequency nature of the impedance measurements used in sensor diagnostics, it was deemed that any mass loading effects of being submerged in the liquid nitrogen would be negligible, as compared to the dynamic tests of the previous study.

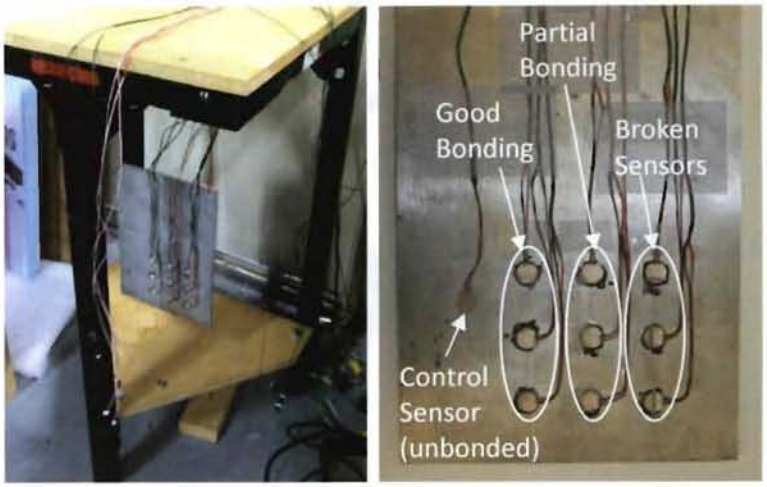

Figure 6: Test setup used to investigate sensor diagnostics at cryogenic temperatures. Ten sensors were investigated: one control sensor, three with good bonding, three with partial bonding, and three that were intentionally broken.

Data for this series of experiments was collected using an Agilent 4294A Precision Impedance Analyzer. Samples were interrogated with a 0.5V chirp signal from 1,000 – 20,000 Hz, and the electrical impedance response was monitored. Two sets of data were taken for cycle to ensure that any anomalies can be identified during the testing procedure. Following the measurement the imaginary component of the admittance signal was extracted in MATLAB to study how the PZT bonding condition evolves with each thermal cycle .

5. EXPERIMENTAL RESULTS

The experimental studies that were conducted as part of this investigation were carried out over a period of three weeks at the NHMFL facility at LANL. The first experiments were designed to identify the most reliable adhesive for use in subsequent experiments. Once this adhesive had been identified, experiments focused on the performance of FBG and RFSG sensors given low frequency, pseudo-static loads were conducted. Dynamic studies followed these in which RFSG, PVDF, and PZT were evaluated. The final series of experiments focus the application of sensor self-diagnostics at cryogenic temperatures.

5.1 Adhesion at Cryogenic Temperatures

The criteria for a suitable epoxy proved to be quite specific, as an epoxy withstanding cryogenic temperatures is crucial. Additionally, bonding integrity when submerged in a liquid environment was also necessary. Figure 7 illustrates the dynamic response of RFSGs bonded to a 304 stainless steel substrate using two of the principal adhesives considered in this study: MBond and Stycast ES-2-20 Epoxy. MBond adhesive was selected due to its wide use in strain gauge mounting, whereas the Stycast epoxy was selected due to recommendations from staff at the NHMFL facility. The benefit of the Stycast epoxy at cryogenic temperatures is that it is doped with fine aluminum particulates which provide thermal expansion properties that are relatively consistent with metallic substrates. The thermal expansion properties help to limit some of the debonding issues observed with some other adhesives. One issue that was observed with the Stycast epoxy was a relatively high viscosity relative to the baseline MBond adhesive. From the results shown in Figure 7, it is seen that the samples prepared with Stycast were not adversely affected by the higher viscosity, as the sensitivities are nearly identical with those of the MBond samples.

One issue that was evident throughout these experiments was the need for a systematic bonding procedure, particularly for samples with polymeric coatings, such as the PVDF sensor shown in Figure 8. The bonding procedure that was developed as part of this study was to roughen the sensor and substrate surfaces to be bonded, cleaning the surfaces with alcohol prior to bonding, allowing the surfaces to dry, and then applying the adhesive and uniform pressure over the sensors entire area for several hours.

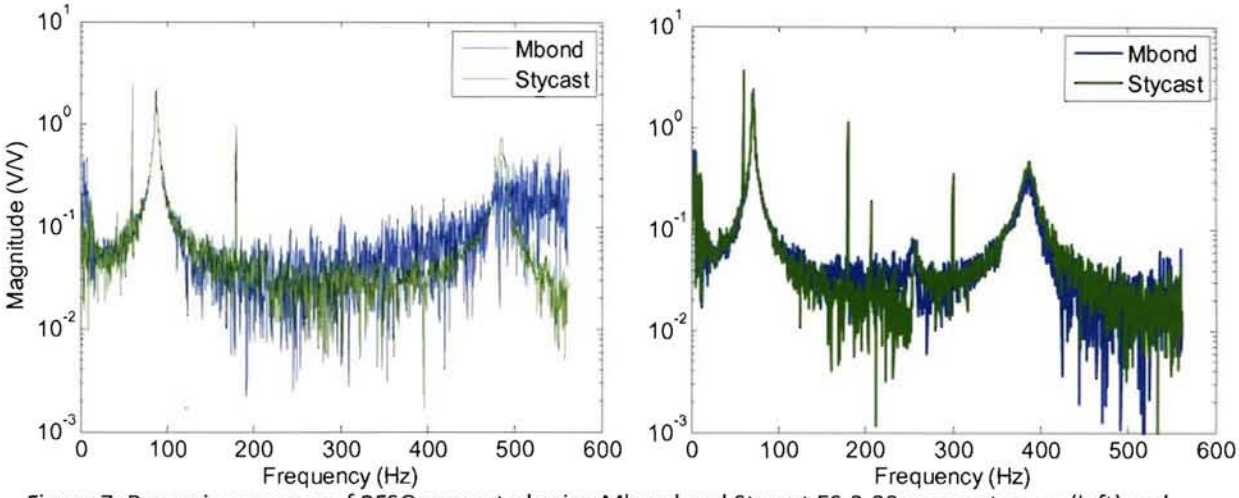

Figure 7: Dynamic response of RFSGs mounted using Mbond and Stycast ES-2-20 epoxy at room (left) and cryogenic (right) temperatures. Both adhesives performed well when substrates were properly prepared.

Additionally, the sensor wires were taped to the substrate to provide a strain relief to further protect the sensors when submerged in the liquid nitrogen bath. This bonding procedure was utilized for each of the flat sensors used throughout the remainder of these experiments.

5.2 FBG and RFSG Response to Static Deformations

Due to bandwidth limitation with the Micron Optics sensing equipment, experiments were limited to pseudo-static deflections below 1 Hz in the FBG characterization. For comparison purposes a resistive foils strain gauge was mounted on the opposing face of the 304 stainless steel sample beam as shown in Figure 9. Room temperature tests were first performed to compare the sensitivity of the FBG with that of the RFSG, using an adjustment screw to impose pseudo-static deformations from 0-4mm in 0.8mm intervals. The results of this room temperature test are shown in Figure 10. There is good general agreement in the shape of the FBG and RFSG responses; however there are some discrepancies when the sample is relaxed and as it nears a peak deformation of 4mm at the center of the sample. Several possible sources for the deviation between the RFSG and FBG are bond integrity/relaxation and the additional strain imposed by solder joints and wiring on the RFSG. Further testing will be needed to identify the source of this variation between the two sensors at room temperature. The more interesting result; however, is the RFSG response at Cryogenic temperatures. As these tests were not to be

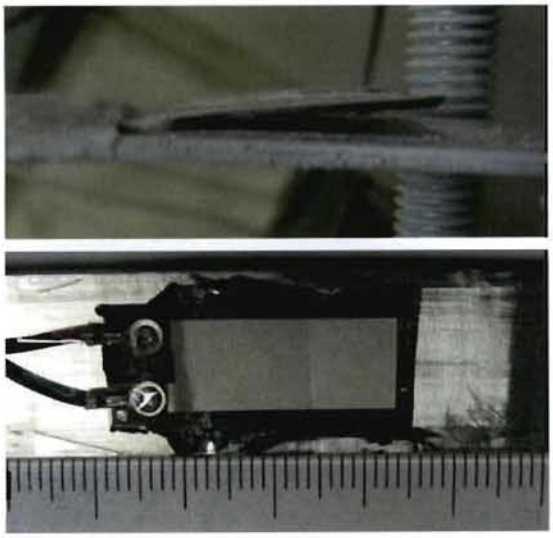

Figure 8: Debonding observed in PVDF sensors during testing.

Figure 9: Resistive foil strain gauge and fiber Bragg grating mounted to the stainless steel substrate.

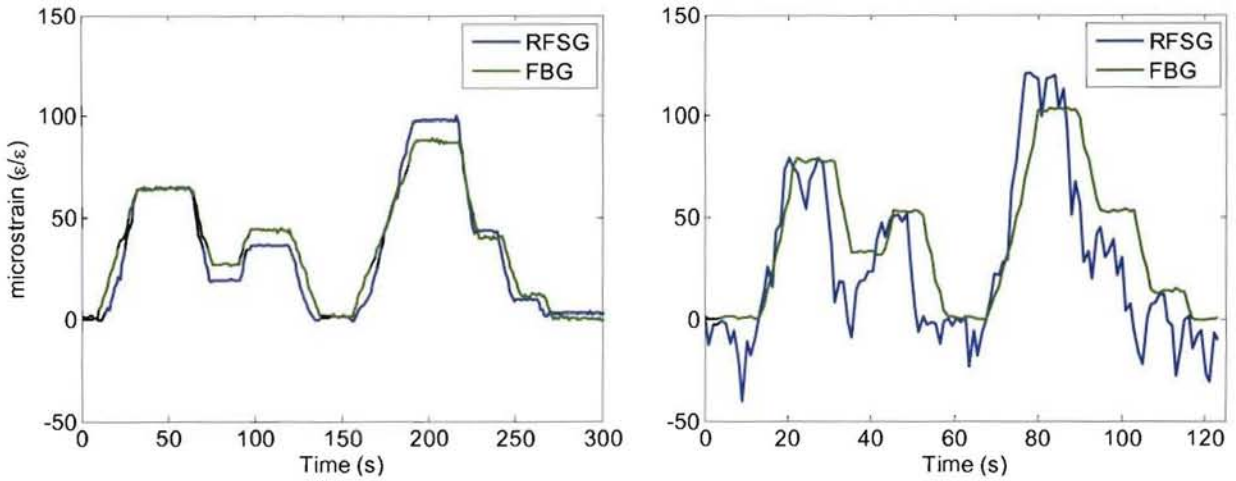

Figure 10: Strain response measured by RFSG and FBG sensors at room (left) and cryogenic (right) temperatures.

conducted at any appreciable strain rates, the tests were conducted with the sample submerged in liquid nitrogen throughout the duration of the experiment. It can be seen that the FBG provides very consistent strain measurements, similar to those observed at room temperature, whereas the RFSG response follows a similar trend yet includes much more variability than it did at room temperature. This sporadic behavior is attributed to a partial debonding in the resistive foil strain gauge during the cooling process. As the majority of the RFSG remains bonded to the substrate, the overall shape of the strain response follows that of the FBG, however, turbulence in the liquid nitrogen is reflected in the response as it imparts dynamic strains in the unbonded section of the RFSG.

One issue that was encountered throughout the static testing was the fragility of the FBG sensors, particularly when being submerged in the LiN bath. Several sensors were damaged during installation and testing, and due to limited resources only one of the FBG sensors could be fully tested at both room temperature and in the cryogenic environment. Further tests need to be performed to fully correlate the response of the RFSG with that of the FBG at cryogenic temperatures.

5.3 Dynamic characterization of RFSG, PVDF, and PZT sensors

Following the static comparisons of the resistive foil strain gauge and the fiber Bragg grating, the dynamic response of the RFSG was considered, along with that of the piezoelectric polymer PVDF and the piezoceramic PZT sensors. In Figure 11 the dynamic response of the three sensing materials are

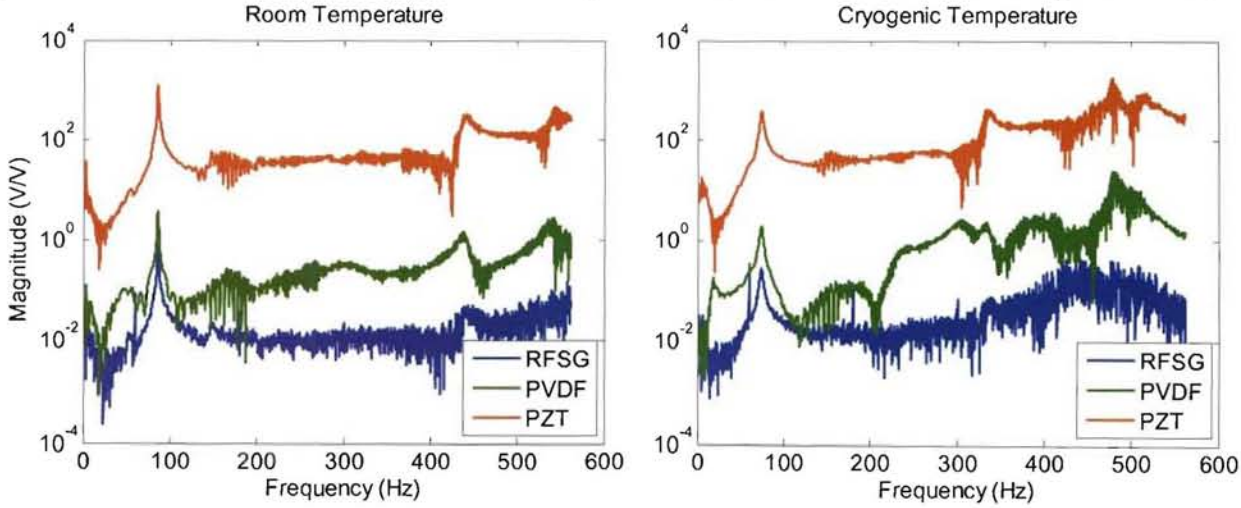

Figure 11: Comparison of the dynamic response of RFSG, PVDF, and PZT sensors for a fixed-fixed stainless steel substrate at room (left) and cryogenic (right) temperatures.

illustrated at both room and cryogenic temperatures. It is evident from the results in Figure 11 that the PZT sensor provides the largest sensitivity to strain, followed by the PVDF and RFSG sensor. Limitations on the RFSG at higher frequencies may, however, be attributed to the Vishay signal conditioning hardware that was being used. It can also be seen from the figure that cryogenic temperatures influence the sensitivity of each transducer, particularly near the first natural frequency of the fixed-fixed beam sample. In addition, initial tests demonstrated the influence of the liquid nitrogen on test results.

As part of this test, samples were evaluated in three different conditions, 1.) at room temperature (in open air), 2) submerged below the liquid nitrogen bath, and 3.) suspended 30mm above the LiN bath after it had been submerged for 10 minutes. The results of this comparison are presented in Figure 12. It is clear that the LiN served to mass load the test sample by lowering the 1st natural frequency by 15%. It also is evident that the fluid served to increase damping in the system as evident in the frequency response results of Figure 12. When removed from the LiN bath the amplitude of the 1st natural frequency returned to a level near that measured at room temperature for the PZT and RFSG samples, however this was not the case for the PVDF sensor. This deviation in the PVDF sensor is attributed to severe debonding in the sensor, as illustrated in Figure 8. In addition to the loss in performance of the PVDF sensor, it is also noted that the natural frequency at cryogenic temperatures is actually lower than that for the room temperature results. This is counterintuitive to the fact that the substrate contracts at colder temperatures, and thus should exhibit an increase in its first natural frequency. Further investigation indicates that this lowering in frequency can be attributed to the clamping mechanism used to apply the fixed-fixed boundary conditions. It was observed during testing that the clamping condition actually loosened upon cooling, thus relaxing the boundary condition and thus causing the natural frequency to drop.

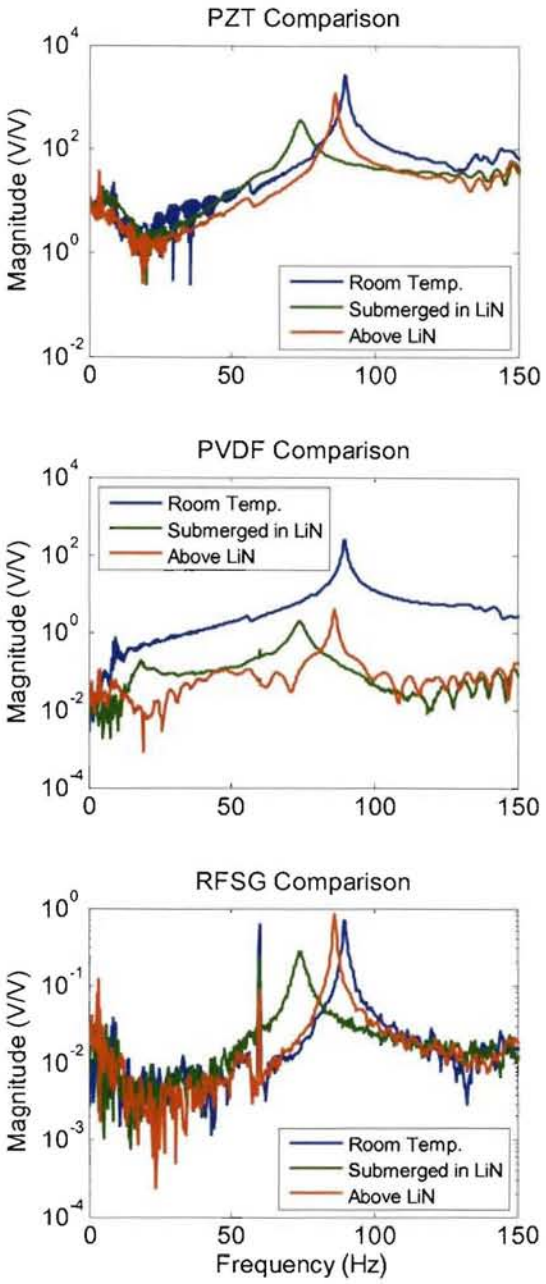

Figure 12: First natural frequency response for PZT (top), PVDF (middle), and RFSG (lower) samples at room temperature, submerged in liquid nitrogen, and suspended above liquid nitrogen

To investigate this issue further a series of free-free experiments were conducted to examine how the boundary condition influences the system's first natural frequency. For the free-free experiment the sample was mounted to the stinger attachment through the center hole as shown in Figure 13. The results of this study for the 304 stainless steel sample are shown in Figure 14. As stated previously, a chirp signal from 10-1000 Hz was used to excite the beam at room temperature. In Figure 14, the graph depicts a very slight difference in the frequency of the first bending mode, though the second bending mode is less apparent at up to 600 Hz in the fixed-fixed structure. From this response it can be seen that the free-free condition does has a lower 1st natural frequency as expected, however it is only a reduction of 3%, whereas the cryogenic temperature produced a reduction of approximately 5%. Further tests will need to be conducted to determine why the cryogenic

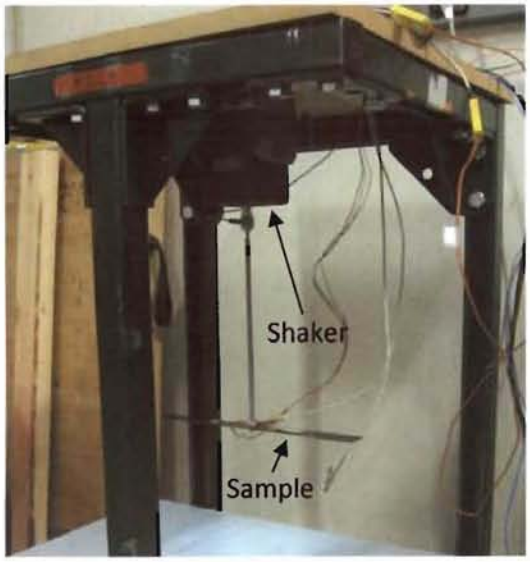

Figure 13: Testing apparatus used in the free-free test configuration.

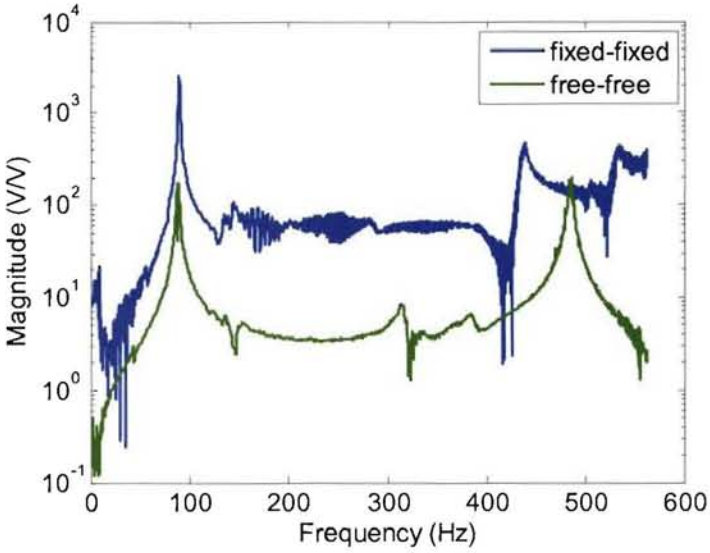

Figure 14: Comparison of the dynamic response measured by a PZT sensor for fixed-fixed and free-free boundary conditions.

temperature produces such a noticeable shift in the natural frequency, particularly since the shift is larger than that observed between the fixed-fixed and free-free conditions.

5.4 Sensor diagnostics

Another advantage of the PZT sensor, in addition to its high sensitivity, is that it can be used to apply high frequency structural health monitoring (SHM) approaches to a structure, as well as its ability to interrogate the bond integrity between the sensor and the substrate, a process referred to as sensor self-diagnostics. In SHM applications it can be difficult to ascertain whether an anomalous results is related to structural or sensor related damage. The objective of performing this series of initial sensor diagnostics experiments is to characterize the response of likely modes of damage in sensors at room and cryogenic temperatures. The results of these tests could later be used to distinguish between sensor and structural damage should piezoelectric sensors be selected as possibilities for monitoring the health of pulsed magnets. This application is especially relevant to the measurement of strain in high field pulse magnets as any potential sensor network embedded within a high pulse magnet for SHM will likely be inaccessible, and the cycling of a cryogenic harsh environment will likely make sensor damage and debonding a real issue.

As described in the experimental procedure section, an array of nine PZT sensors was mounted on a 5mm thick aluminum plate. The patches are divided into three groups of three. The first series of three gauges were all properly bonded with Stycast epoxy. The second series of three gauges were intentionally partially debonded; wax paper was used under half the gauge so that the epoxy only affixed half of the sensor. The third series of gauges were intentionally damaged; a saw was used to cut the gauges at a 1/4, 3/8, and 1/2 diameter across. A tenth

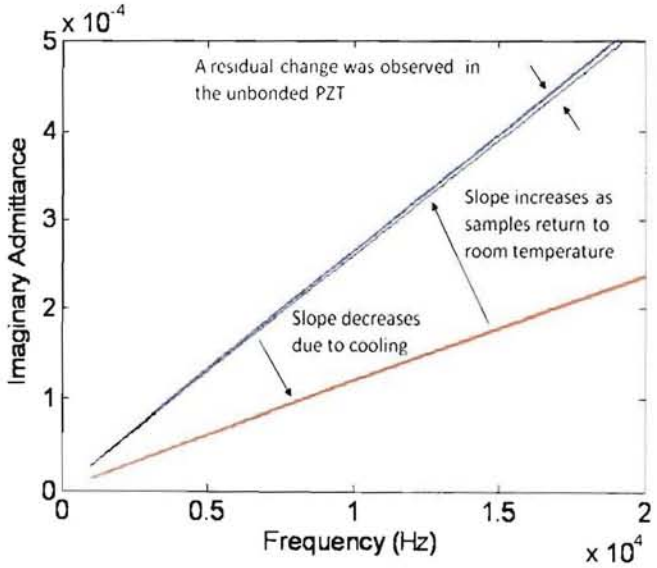

Figure 15: Electrical admittance measurements of a free PZT sensor before, during, and after submersion in liquid nitrogen.

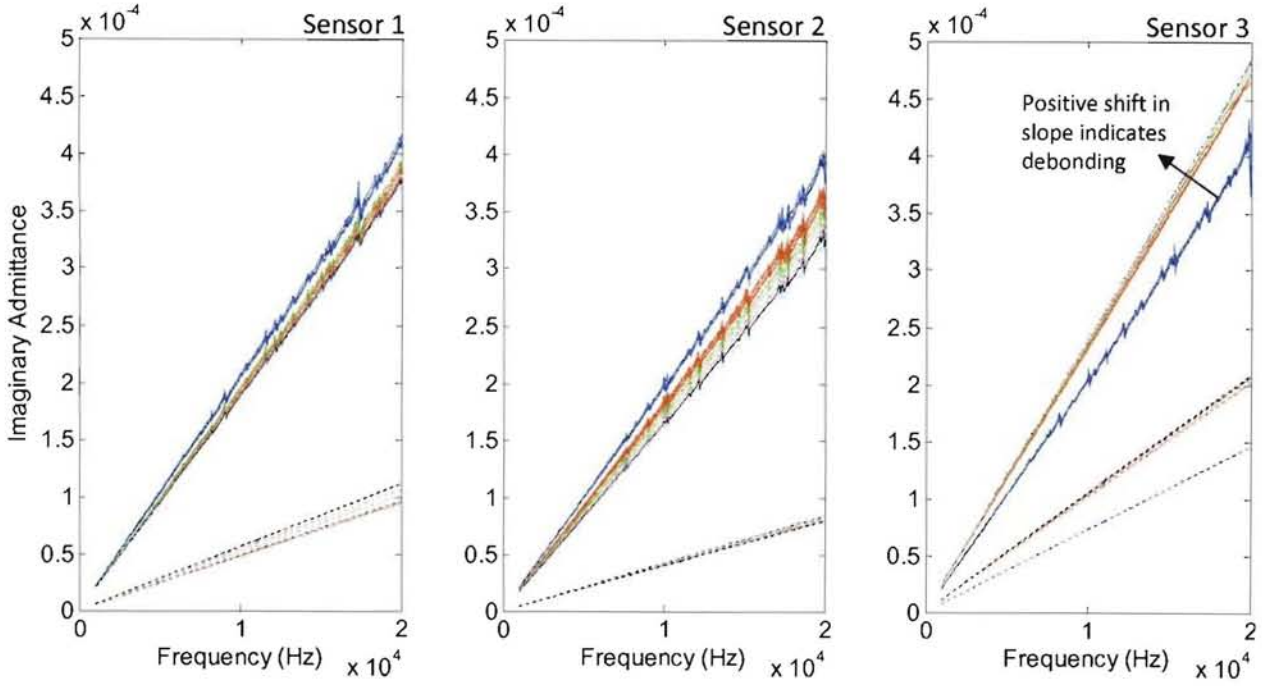

Figure 16: Electrical admittance measurements of sensors that were completely bonded to the aluminum plate.

gauge was used as a baseline, and was not bonded to the plate. Figure 15 presents the results for the baseline sensor as the PZT was cycled from room temperature to 77K and back to room temperature. It is evident that the cryogenic environment greatly influences the sensitivity of the PZT as indicated by the significant change in slope; however, it is most important to note that there is a residual change in the room temperature response of the piezoelectric. Bond integrity is denoted by the slope of this admittance curve, and would need to be monitored relative to a baseline measurement to properly account for the temperature induced shift that is apparent in Figure 15. In general terms, the unbonded piezoelectric sensor will have the greatest slope as the slope is related closely to the electrical capacitance of the PZT. As the sensor is bonded to a substrate, the electrical impedance becomes coupled to the mechanical impedance of the structure through the bonding layer. The mechanical boundary condition imposed by the structure through the bonding layer serves to reduce the electrical capacitance of the PZT, resulting in a decrease in the slope of the admittance. If a sensor is properly bonded to a structure, then a positive change in slope will be indicative of debonding, as the sensor begins to gain capacitance due to a relaxation in the boundary condition. Conversely, damage to the sensor will reduce the overall physical size of the remaining 'operable' region, resulting in a loss of capacitance. Thus, damage to the sensor will generally be reflected as a decrease in slope as the overall electrical capacitance drops. The three sample sets used in this study configured to help illustrate this behavior, and to prove the technique's effectiveness at cryogenic temperatures.

The first series of piezoelectrics (sensors 1-3) were applied to the aluminum substrate using consistent bonding techniques, and are considered to constitute a 'good' bonding condition. Figure 16 presents the admittance curves for each of the sensors throughout the five cycles between room and cryogenic temperatures. The initial room temperature measurement through this discussion is presented as the blue set of curves. It is apparent from these results that the residual shift in slope continues to accumulate throughout the subsequent cooling cycles. While this is a feature that appears to be related to the sensor itself, it is a behavior that will need to be investigated further before the long term deployment of these sensors could be undertaken in applications where large thermal cycles would be expected. One of the more interesting results of Figure 16 relates to sensor 3. Based upon the response it is seen that the sensor underwent some debonding during the first warming cycle as the plate was brought back to room temperature following the first submersion in LiN. This debonding is evident in the positive change in slope; however, following this first instance of debonding, the sensor behaved consistently throughout subsequent cooling cycles. Additionally, the admittance response to debonding is apparent in

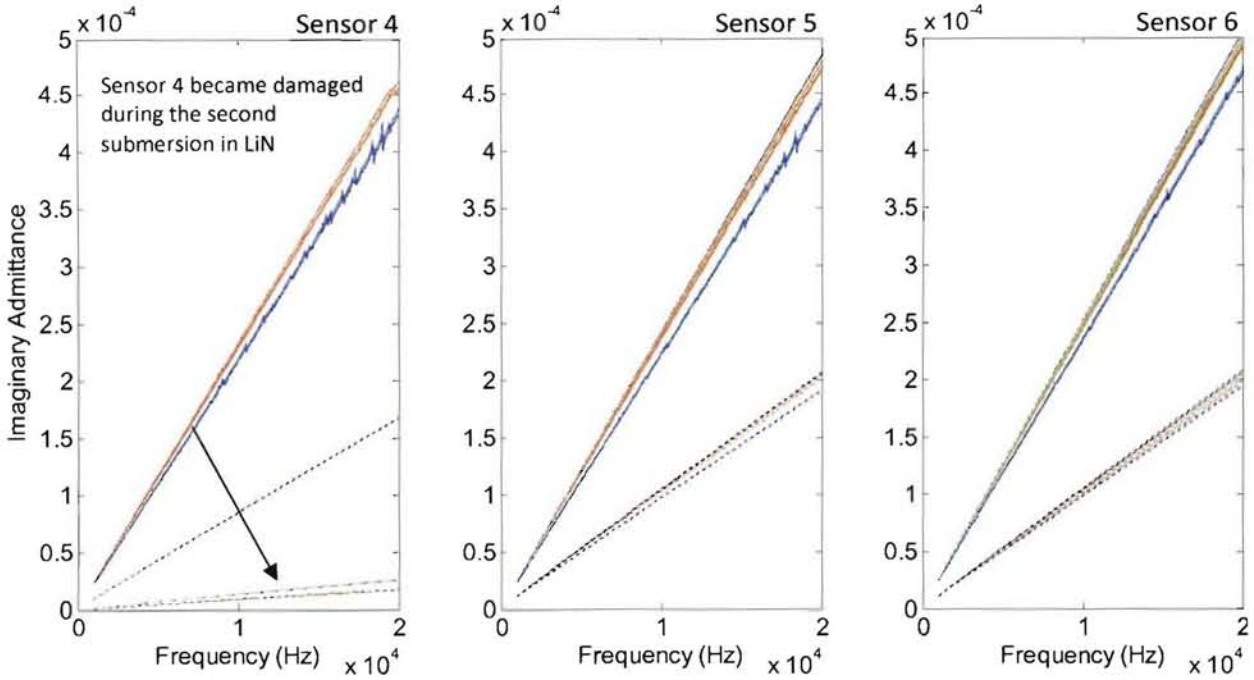

Figure 18: Electrical admittance measurements sensors that were partially bonded to the aluminum plate.

both room temperature and cryogenic data sets, as the positive change in slope is present in both temperature regimes.

The second series of PZTs (sensor 4-6) were partially bonded to the aluminum substrate using wax paper to prevent adhesion of 1/4, 1/2, and 3/4 of the sensor diameter. This change in bonding area can be seen in the solid blue admittance curves of Figure 17. One interesting feature of this series of curves is that the residual shift in admittance values is in the positive direction, rather than the negative direction as seen in the baseline sample. This behavior is attributed to the fact that the partial bonding condition serves to constrain the PZT in a pseudo-cantilevered configuration. In such a configuration it is assumed that the impedance measurement itself causes the sensor to deform as a voltage signal is applied to the PZT, progressively deteriorating the bond, giving rise to subsequent debonding with each measurement at the interface with the wax paper. X-ray or imaging analysis should be conducted to provide support of this assumption.

In addition to the residual changes in the admittance curve, it is also interesting to observe the change in response exhibited by sensor 4 in Figure 17. During the first submersion cycle the sensor behaved as the other two sensors did; however, on the second submersion it is seen that the sensor suffered some damage. Upon completion of the tests, visual inspection found that there was a significant crack that developed in the sensor along the solder joints of the PZT as seen in Figure 18. And, as in the case with sensors 1-3, this characteristic was observed in the data collected at room and cryogenic temperatures.

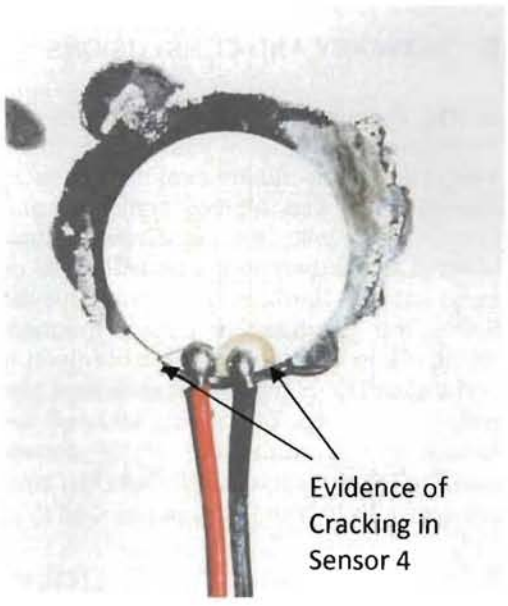

Figure 17: Image of Sensor 4 following the damage induced during the cooling cycle. A crack is evident just above the solder joints.

The final series of PZTs (sensors 7-9) were bonded to the substrate in a consistent manner, then damage was induced using an abrasive cutting tool. Varying degrees of damage

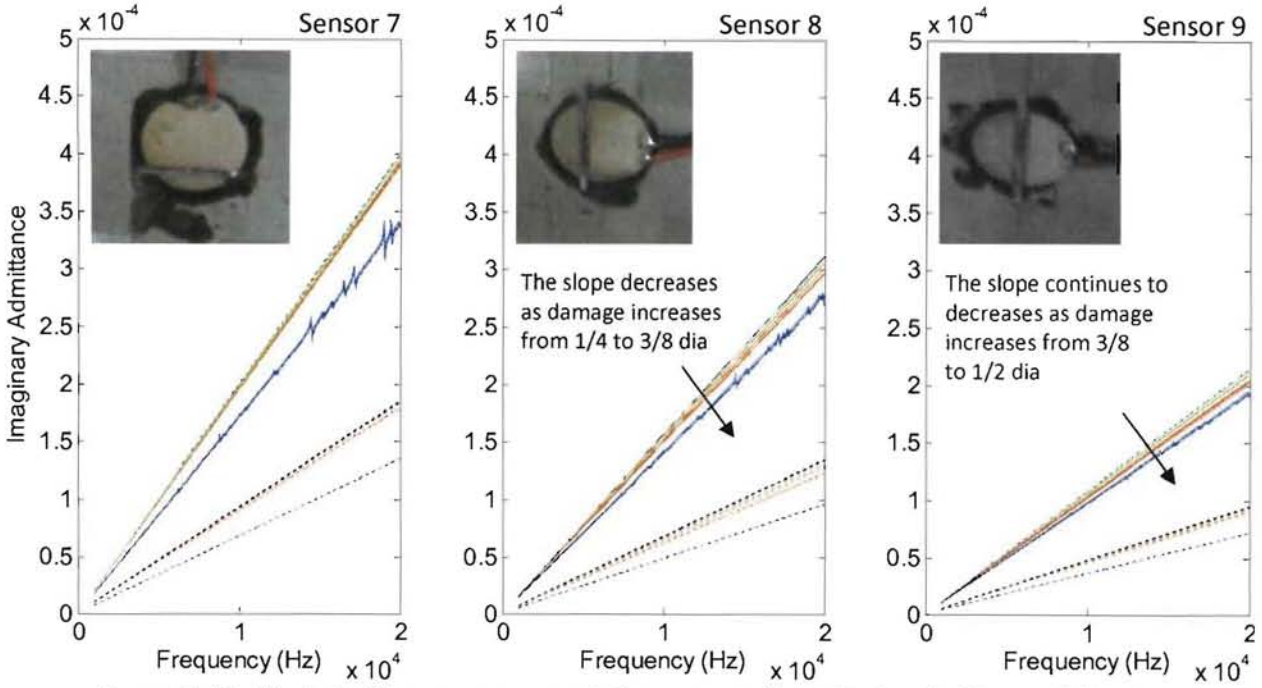

Figure 19: Electrical admittance measurements for sensors with varying levels of imposed damage.

were inflicted on the sensors, detaching 1/4, 3/8, and 1/2 diameter sections. The results obtained from these damaged sensors are shown in Figure 19. It is evident from this figure that the more significant damage produces a significant reduction in the slope of the electrical admittance as is expected from Equations 1-2, and this reduction in slope can be seen in both room temperature and cryogenic datasets. Another feature of this data that should be commented on is the residual increase in slope throughout the cooling cycles. As in the previous case this is counter to what was observed with the baseline PZT, however it is attributed to changes in the bond layer introduced when damage was inflicted on the samples. While this is currently only a hypothesis of what happened, future tests in which damage is inflicted before bonding should help to clarify what is being seen.

5. SUMMARY AND CONCLUSIONS

In this investigation a series of strain sensing technologies have been investigated under cryogenic conditions. The goal of this study is to aid in the identification of a suitable sensing approach that can be integrated within future designs of the high field pulsed magnets at the National High Magnetic Field Laboratory at Los Alamos National Laboratory. Tests indicated that fiber optic sensors provide clear strain signals with little noise when submerged in liquid nitrogen. The fiber optic interrogation hardware used in this experiment was limited to dynamic ranges below 1Hz, and future tests should incorporate more capable hardware that can achieve the higher bandwidths (> 1000Hz) needed to identify anomalies during the operation of pulsed magnets. Piezoelectric ceramics were seen to provide the highest sensitivity to strain of the sensors used in this study. They also provide a much larger dynamic range, and the ability to implement structural health monitoring algorithms and sensor diagnostics techniques to provide high resolution inspection of reinforcement shells as well as the bond integrity between the sensor and the substrate. PVDF sensors also provided high sensitivity measurements, however they were generally plagued with bonding issues, as the mylar protective coating was difficult to bond to, and submersions in liquid nitrogen tended to cause sensors to debond.

While this study has provided a first step in identifying suitable sensors for the NHMFL application, additional work must be undertaken to understand how each sensor responds to the large magnetic fields and eddy currents induced during the pulse cycle of these large scale magnets. Electromagnetic interference may prove to be the deciding factor in selecting a suitable sensing technology. Future studies will be designed to focus on these issues, and to select the most appropriate sensing technology.

References

1. Sims, J.R., Rickel, D.G., Swenson, C.A., Schillig, J.B., Ellis, G.W., and Ammerman, C.N., "Assembly, Commissioning and Operation of the NHMFL 100 Tesla Multi-Pulse Magnet System" in *IEEE Trans. Appl. Supercond., vol. 18, NO. 2, June 2008*
2. Sims, J.R., Schillig, J.B., Boebinger, G.S., Coe, H., Paris, A.W., Gordon, M.J., Pacheco, M.D., Abeln, T.G., Hoagland, R.G., Mataya, M.C., Han, K., and Ishmaku, A., "The U.S. NHMFL 60 T Long Pulse Magnet Failure" in *IEEE Trans. Appl. Supercond.*, vol. 12, no. 1, March 2002.
3. Swenson, C.A., Gavrilin, A.V., Han, K., Walsh, R.P., Schneider-Muntau, H.J., Rickel, D.G., Schillig, J.B., Ammerman, C.N., and Sims, J.R., "Performance of 75 T Prototype Pulsed Magnet" in *IEEE Trans. Appl. Supercond., vol. 16, no. 2, June 2006*
4. Evans, J. E., Dulieu-Barton, J.M., Burguete, R.L., "Electrical Resistance Strain Gauges," *Modern Stress and Strain Analysis,* pp. 4,5. 2009.
5. Evans, J. E., Dulieu-Barton, J.M., Burguete, R.L., Optical Fibre Bragg Grating Strain Sensors," *Modern Stress and Strain Analysis,* pp. 2,3. 2009.
6. Kashyap, R., "Fiber Bragg Grating Band-Pass Filters" in *Fiber Bragg Grating,* no. 2 pp. 237-245, 2004.
7. Park, G., Farrar, C.R., Rutherford, A.C., Robertson, A.N., "Piezoelectric Active Sensor Self-Diagnostics Using Electrical Admittance Measurements" *Journal of Vibration and Acoustics* AUGUST 2006, Vol. 128 / 469
8. Saint-Pierre, N., Jaye, Y., Perrissin-Fabert, I., and Baboux, J. C., "The influence of bonding defects on the electric impedance of a piezoelectric embedded element," *Journal of Physics D: Applied Physics* **29**, pp. 2976–2982, December 1996.
9. Giurgiutiu, V., Zagrai, A. N., "Embedded self-sensing piezoelectric active sensors for on-line structural identification," *Transactions of the ASME* **124**, pp. 116–125, January 2002.
10. Pacou, D., Pernice, M., Dupont, M., and Osmont, D., "Study of the interaction between bonded piezo-electric devices and plates," in *1st European Workshop on Structural Health Monitoring*, (155), 2002.
11. Bhalla S., and Soh, C.K., "Electromechanical impedance modeling for adhesively bonded piezo-transducers," *Journal of Intelligent Material Systems and Structures* **15**, pp. 955–972, December 2004.
12. Park, G., Farrar, C. R., di Scalea, F. L., and Corria, S., "Performance assessment and validation of piezoelectric active-sensors in structural health monitoring," *Smart Materials and Structures* **15**, pp. 1673–1683, December 2006.

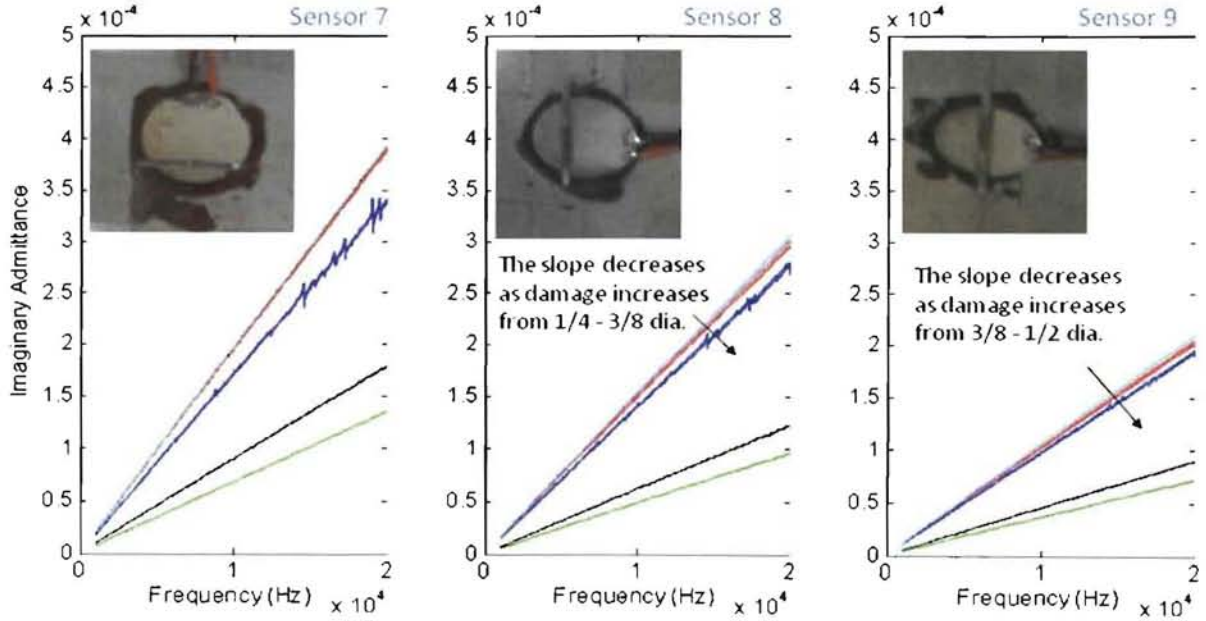

Figure 20: Electrical admittance measurements for sensors with varying levels of imposed damage.